Atomic Force Microscope Nanomanipulation with Simultaneous Visual Guidance

Suenne Kim, Daniel C. Ratchford, and Xiaoqin Li*

Department of Physics, Center for Nano- and Molecular Science and Technology, University of Texas at Austin, Austin, Texas 78712

ARTICLE

ABSTRACT Atomic force microscopy (AFM) has been used to assemble prototype nanostructures consisting of colloidal nanoparticles. In the standard manipulation protocol, the AFM is used either as a manipulation tool or an imaging tool, but not both at the same time. We developed a new nanomanipulation protocol in which simultaneous visual guidance is obtained during manipulation. As an example, Au nanoparticles were manipulated on a substrate in two steps. First, a nanoparticle is kicked with the z feedback off. This kicking event reduces the static friction. Second, the nanoparticle is dribbled to a target position in tapping mode, and visual guidance is provided by a ghost trace of the nanoparticle. The new manipulation protocol greatly improves efficiency of manipulating small nanoparticles (15 nm in diameter or smaller). Our work highlights the importance and challenges of understanding friction at the nanoscale.

KEYWORDS: atomic force microscopy · nanomanipulation · colloidal nanoparticles · friction · visual guidance

Scanning probe microscopy (SPM) can be used not only to characterize but also to modify surfaces with atomic resolution.[1−6] While the capability to manipulate individual atoms is impressive, manipulating objects with diameters ranging from a few nanometers to tens of nanometers in ambient environments poses its own challenges and has broad applications in nanotechnology. For example, one can use SPM to assemble prototype nanostructures consisting of metallic and/or semiconductor nanoparticles (NPs). Many intriguing types of nanostructures and superstructures have been successfully synthesized in solutions. These new materials have tremendous potential for new functionalities and properties such as surface-enhanced Raman scattering and negative index of refraction.[7] However, solution-based syntheses of nanoclusters typically produce a broad range of species. The production of a specific type of nanostructure with high yield is very challenging. Relying on nanomanipulation, one can assemble "designer" nanostructures with well-controlled composition and geometry. The development of an efficient nanomanipulation method will provide an exciting opportunity to study these well-controlled structures individually.

Atomic force microscopy (AFM) is well suited for nanomanipulation tasks. Much progress has been made in the past decade in the area of nanomanipulation with AFM. Typically, nanosize objects of various shapes (*e.g.*, spheres, rods, wires, and tubes) were manipulated on a flat substrate.[8−17] Simple three-dimensional manipulations, such as pushing a NP across a step or over other particles, have been demonstrated.[8,18] Automatic manipulation protocols have been devised and implemented with some success.[8]

Despite many remarkable accomplishments in this area, nanomanipulation methods remain time-consuming and inaccurate. The difficulty lies partially in the lack of simultaneous visual guidance during the manipulation process. In a few previous studies, simultaneous visual guidance during manipulation was provided by operating a manipulator inside the chamber of a scanning electron microscope or a specialized home-built instrument.[19−22] Such approaches often require tedious sample preparation procedures and impose limitations on the types of samples that can be investigated.

In a standard manipulation protocol, the NP is first imaged with the feedback engaged. Next, the z feedback is turned off. The tip is moved in a straight line through the center of the NP to push the NP upon contact. Once a target position is reached, the feedback is re-engaged, and the NP stops moving. Finally, the sample is imaged again to examine the result of the manipulation. In this standard protocol, the AFM is used either as a manipulation tool or an imaging tool, but not both at the same time. If a particle is not struck directly

*Address correspondence to elaineli@physics.utexas.edu.

Received for review June 9, 2009 and accepted September 8, 2009.

Published online September 14, 2009.
10.1021/nn900606s CCC: $40.75

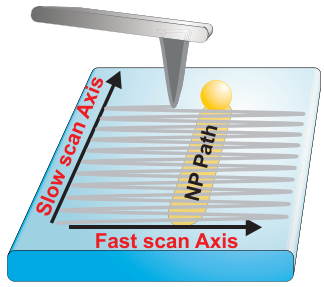

Figure 1. An illustration of the new manipulation method. Following an initial kicking event, the static friction is reduced. One can then move the NP in tapping mode at a high scanning rate. The NP moves in a direction perpendicular to the fast scanning axis. A trace of ghost images is left along the path, providing visual guidance during manipulation.

in its center, the particle can easily slip away from the tip and the manipulation would fail. Usually the user can only find out the result after taking the second image.[8] Therefore, manipulation of small NPs over long distances can be very time-consuming. The associated technical difficulties originate from the spatial uncertainties caused mostly by thermal drift or nonlinearities of piezo actuators such as hysteresis and creep.[8]

Certain empirical rules of friction still hold in the mesoscopic regime. It is well-known that static friction is larger than kinetic friction. A less-known, yet very important rule is that static friction increases the longer two surfaces stay in stationary contact.[23] On the basis of these simple rules of tribology, we demonstrate a novel nanomanipulation protocol, which works effectively even in the presence of spatial uncertainties caused by piezo-actuators and drift. There are two distinct steps of manipulation in this new method. In the first step, one kicks a chosen NP using the standard method in a random direction and distance. The static friction is greatly reduced following this initial movement. In the second step, one can manipulate the NP controllably in tapping mode with the feedback engaged because of the reduction in static friction following the first step. If the scanning rate exceeds a threshold value, the NP starts to move in the direction perpendicular to the fast scanning axis, as illustrated in Figure 1. Once the target position is reached, the scanning rate is abruptly reduced well below the threshold value, and the NP stops moving. There are two main advantages to this technique: (1) it is not necessary to strike the NP on its centerline to push it, and (2) visual guidance *in situ* can be obtained during the manipulation. Thus the new method greatly reduces the manipulation time and increases the success rate of long-range manipulation, especially when one manipulates NPs of small sizes.

RESULTS AND DISCUSSION

We demonstrate how to controllably move a NP by adjusting the scanning speed and using visual guidance in the first example. We prepared 15 nm Au NPs on a quartz substrate with ~2 nm surface roughness. A small area (1 μm × 1 μm) was scanned before any manipulation had taken place (Figure 2a). We chose the NP particle enclosed in the arrow mark to manipulate. Our goal was to place it along the same horizontal axis as a pair of NPs in the middle of the image plane (enclosed in a blue circle). The tip was fast scanned along the horizontal axis and moved from the bottom to the top of the image plane so that the NP could be pushed upward. After kicking the NP using the standard method, the scanning speed was increased in steps from Figure 2b to 2d to find the threshold scanning rate for dribbling the NP. The NP (enclosed in the yellow ellipse) was moved at scanning rates of 1 Hz (Figure 2b) and 5 Hz (Figure 2c), but did not reach the target position. When the scanning rate was increased to 7 Hz, the chosen NP moved controllably.[24] To stop the particle at the target position, as shown in Figure 2d, we abruptly reduced the scanning rate to 1 Hz. While we presented several consecutive images with gradually increasing scanning rates in Figure 2b−d, the user can always choose a higher scanning rate (~15 Hz) to ensure a high success rate in manipulation.

One can observe a track of ghost images in Figure 2b−d along the path of the moving NP. These ghost images, also illustrated in Figure 1, provide easily recognizable visual guidance. The track appears because the

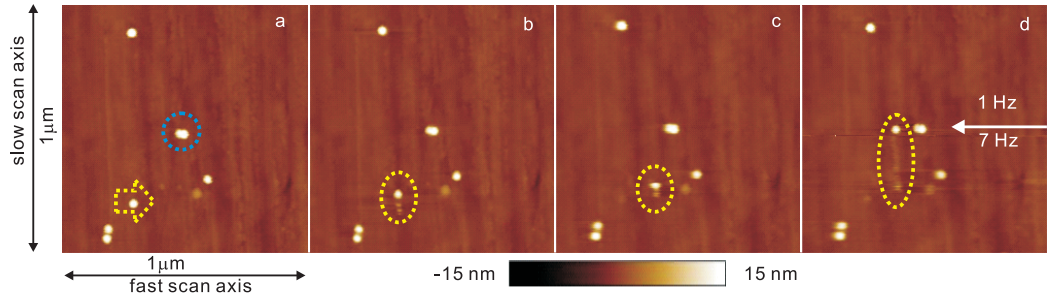

Figure 2. Nanomanipulation with visual guidance. (a) An image taken at 1 Hz before any manipulation. The NP enclosed in the arrow mark was kicked to the right using the standard method. Following the kicking event, images were taken at a scanning speed of (b) 1 Hz and (c) 5 Hz. In both cases, the NP enclosed in the circles moved a short distance but stopped before reaching the target position. (d) Controlled manipulation was achieved at a higher scanning rate of 7 Hz. The scanning speed was abruptly reduced from 7 to 1 Hz once the target position was reached. Ghost images behind the moving particle provide a useful and clear visual guidance during the manipulation.

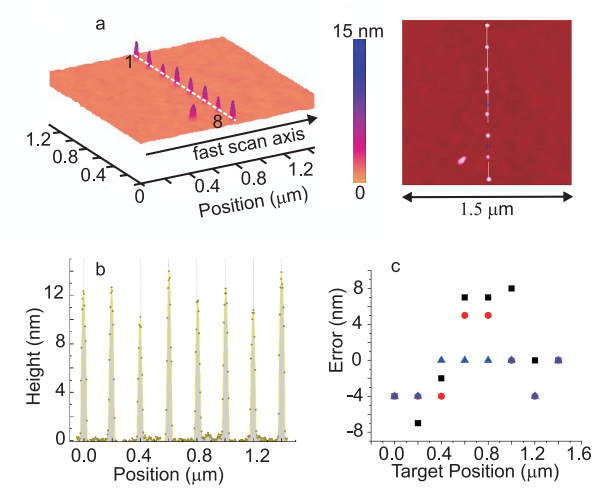

Figure 3. (a) The 3D and 2D views of a network of 8 NPs assembled in a straight line. (b) The cross-section profile of the assembled NPs along a line cut. (c) Errors represent the deviations of the NPs' positions from the target spacing of 0.2 μm. Different color symbols represent errors extracted from three different line cuts.

tip initially starts to image the particle, but as the tip moves along the fast scan axis, it exerts a force to the NP greater than the resistive force of the reduced static friction. The particle then moves along the slow scan axis. We also note that the only NP moved in the whole scanning area is the chosen particle enclosed in either the arrow in Figure 2a or in the yellow ellipse in Figure 2 b−d. This observation further proves that the first kicking step is critical: the kicking step reduces the static friction so that the chosen NP (and only the chosen one) can be manipulated in tapping mode. Within the static friction build-up time, which ranges from tens of seconds to several minutes, one can continue to manipulate the chosen NP in tapping mode.

In the second example, we manipulated Au NPs on a smooth quartz surface with ~0.5 nm surface roughness. We assembled one line of eight NPs separated each by 200 nm using a combination of the standard and new methods for comparison,[25] as displayed in the 2D and 3D views of Figure 3a. Achieving this goal requires moving small NPs (~15 nm) over long distances, which is very challenging using the standard manipulation protocol. The height and position of each NP are displayed in the cross-sectional profile along a line cut presented in Figure 3b. The variation of the heights results from both the error in manipulation and the size variation of the NPs themselves. The positions of the NPs are determined *via* Gaussian fits to the cross-sectional profile. The errors in the NPs' positions from the target positions are analyzed along three different line cuts and displayed in Figure 3c.

While the measured error of manipulation is comparable between the two methods, we emphasize that the new method is much more efficient due to the visual guidance. In the standard manipulation method, it is important for the tip to push along the centerline of the NP. Identifying the centerline of NPs becomes more difficult as the NP gets smaller. Over long distances, the tip may become easily off-centered during its course. Therefore, one has to take many steps in moving small NPs (~15 nm in diameters or smaller) over long distance (~50 nm or longer).[8] Between each step, a separate image has to be acquired to locate the NP and its centerline. Using the new method, however, once the particle is initially kicked, it is no longer necessary to relocate the center of the NP prior to pushing. Furthermore, one can observe the position of the NP during the manipulation, thus eliminating the need for acquiring images in the intermediate steps. In this example, manipulation time was shortened by approximately a factor of 5−10 using the new method for the 15 nm particles depending on the travel distance.

The new manipulation method takes advantage of the time-dependent nature of the static friction. In the mesoscopic regime, friction is no longer proportional to the normal load. When the load drops below a certain value (~50 μN),[26] one needs to modify the relation as, $F_{\text{friction}}(t) = \mu(t)[N + L_{\text{adh}}(t)]$, which states that friction is proportional to the sum of the normal load and the adhesion.[27] The adhesion force is related to the local environment of the contact area between the NPs and substrate. Both the friction coefficient and adhesion force may increase as a function of time.

A time-dependent double-well potential model can provide some physical intuition for the ability to move NPs in the AFM tapping mode following the kicking.[28]

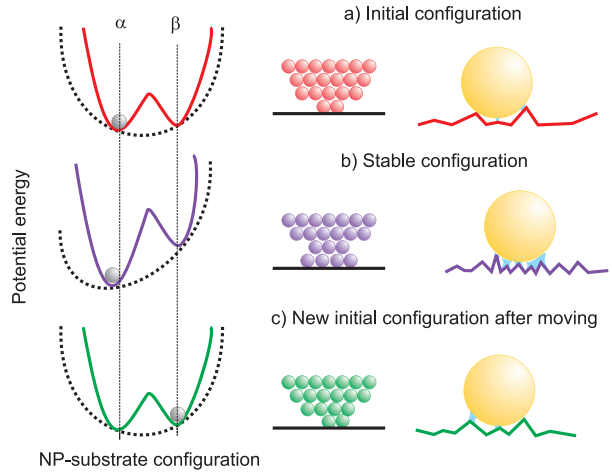

Figure 4. A double-well potential model depicting the NP−substrate configurations in (a) the initial state, (b) the stable state after a long dwelling time, and (c) a new initial state after kicking. The left column depicts that the potential energy of the system changes as a function of NP−substrate configurations. The dashed curve represents a certain constraining condition for the local potential minimum. The middle column describes structural relaxations at the interface as atoms in the NP are rearranged for minimal potential. The right column illustrates the increase in the number of water bridges formed.

As illustrated in Figure 4a, the system may be in a configuration ("α") of local potential energy minimum after initial contact. There are many other equivalent, energetically degenerate configurations represented by "β". Over time, a number of thermally activated processes (*e.g.*, capillary water bridge formations[29] and asperity creep[30]) may lead to small changes in the NP-substrate configurations, subsequent modifications in potential energy landscape, and an increase in friction (Figure 4b). As the energy barrier grows, it becomes increasingly difficult to move the NP out of the more stable configuration in tapping mode. Kicking the NP clears all memory of the previous contact time and resets the system configuration into a new initial state "β" (Figure 4c). Because the energy barrier between different configurations in state "β" remains low shortly after the kicking, one can controllably manipulate the NP in tapping mode.

The time-dependent behavior of static friction between solid surfaces has been extensively studied. We illustrate two processes in Figure 4 that may apply to the particular system under study. First, structural relaxation may occur as atoms in the NPs move to energetically more favorable locations at the junction,[27] modifying the adhesion force and thus friction.[31] We do not exclude the possibility that atoms in the substrate may reposition themselves to accommodate the reconfiguration of Au atoms or that the NP as a whole moves slightly to another position on the substrate. Second, the formation of capillary water bridges may also play a crucial role in nanomanipulation under ambient environments.[29,32] Over time, the number of water bridges formed between the NP and substrate asperities increases, leading to an increased adhesion force and static friction.

Measuring and modeling the magnitude of friction at the nanoscale is a challenging task. In principle, the force exerted by the AFM tip can be measured by monitoring the deflection of the tip in contact mode. In the new nanomanipulation method, however, the AFM is operated in tapping mode. Therefore, we were unable to measure friction directly. We provide an estimate for the order of magnitude of the friction involved in the manipulation process following a simple analytical approach.

Extensive theoretical and experimental studies suggest that friction at the nanoscale is proportional to the actual contact area, that is, $F_{\text{friction}} = \tau A$, where τ is the shear strength.[33] We calculate the contact area on the basis of continuum elasticity theories. Two widely applied analytical theories for deformable spheres considering adhesion have been developed by Johnson, Kendall, Roberts (known as the JKR theory[34]) and Derjaguin, Muller, Toporov, Maugis (known as the DMT-M theory[35]), respectively. It was pointed out by Tabor[36] that these two theories apply in different limits depending on a parameter

$$\eta \equiv \left(\frac{16R\gamma^2}{9K^2z_0^3}\right)^{1/3}$$

where R is the radius of the sphere, γ is the work of adhesion, and z_0 is the equilibrium spacing for the Lennard-Jones potential of the surfaces. K is the combined elastic modulus of the sphere and substrate defined as $K = {}^4/_3[(1 - \nu_1^2)/E_1 + (1 - \nu_2^2)/E_2]^{-1}$, in which $\nu_{1,2}$ and $E_{1,2}$ are the Poisson's ratios and Young's modulus for the substrate and sphere. If η is large ($\eta \geq 5$), the JKR theory applies. If η is small ($\eta \leq 0.1$), the DMT-M theory is more appropriate. Physically, a small value in η describes hard contacts for small spheres.

We have calculated $\eta = 0.07$ assuming the following parameters: $E_{\text{quartz}} = 71.7$ GPa, $\nu_{\text{quartz}} = 0.17$, $E_{\text{Au}} = 78$ GPa, $\nu_{\text{Au}} = 0.44$, $\gamma = 50$ mJ/m^2 (typical value for van der Waals surfaces), $R = 7.5$ nm, and $z_0 = 0.3$ nm. The value of η suggests that DMT-M is more appropriate for our case. We note that the difference between the JRK and DMT-M theory in estimating friction is only about a factor of 2. One can safely ignore gravity in comparison to adhesion force for NPs. Under this condition, the contact area is calculated by

$$A_{\text{DMT-M}} = \pi\left(\frac{2\pi\gamma}{K}\right)^{2/3}R^{4/3}$$

For Au NPs of 15 nm in diameter, the contact area is ~1.5 nm^2. This expression indicates that friction increases with the radius of spheres as $A \propto R^{4/3}$. A previous study aimed to confirm this relation yielded inconclusive results.[22] We suggest that the discrepancy partially arises because the previous study failed to take into account the time-dependent nature of friction.

To obtain an estimated value for the shear strength, τ, we use the relation, $\tau^{\text{theo}} = G^*/30$, between the theoretical shear strength and the combined shear force modulus, $G^* = [(2 - \nu_1)/G_1 + (2 - \nu_2)/G_2]^{-1}$, where $G_{1,2} = E_{1,2}/(2 + 2\nu_{1,2})$.[37,38] Finally, using $F_{\text{friction}} = \tau^{\text{theo}}A_{\text{DMT-M}}$, we obtained an estimated upper bound for friction as 0.4 nN. The simple analytical calculation presented here is based on the elastic deformation of a sphere on a perfectly flat substrate, which likely leads to an overestimated contact area. In addition, the calculation does not include capillary water bridge formation, which is inevitable under ambient environments. The actual value of friction is, of course, time dependent, and critically depends on conditions such as surface roughness. The time dependent nature of friction can be accounted for by the increasing contact area, arising from water bridge formation and structural relaxation, *etc.*

CONCLUSION

In summary, we have demonstrated a new nanomanipulation protocol. The distinctive feature of the technique is to reduce the static friction by giving the NP an initial kick. One can then effectively manipulate NPs with a lateral sweeping force in im-

aging mode. To the best of our knowledge, this is the first demonstration of using a commercial AFM as a controllable manipulation device and an imaging tool simultaneously.[39−42] The access to visual guidance during manipulation greatly improves the accuracy and the efficiency in moving small NPs over long distance. In addition, we proposed a qualitative time-dependent double-well potential model to explain the mechanism of the new manipulation method. Finally, we derived an upper bound for friction following a simple analytical approach. Improvements in nanomanipulation techniques allow one to assemble complex nanostructures in a more efficient and controlled fashion, promoting the development of multifunctional materials and novel nanosized opto-electronic devices.

METHODS

A closed-loop commercial AFM (Vecco-Dimension 3100) at room temperature was used for nanomanipulation. The nanoman software from Veeco was employed, which compensates for hysteresis and drift to some degree. Commercially available cantilevers were used with nominal force constants of *ca.* 5−7.5 N/m. Samples were prepared on quartz substrates (Meller Optics and Boston Quartz) with two different finishes (surface roughness of ∼2 and ∼0.5 nm, respectively). The substrates were cleaned in piranha solution, rinsed with deionized water, and then dried with high purity nitrogen gas. Colloidal Au NPs with 15 nm diameters were purchased from Ted Pella, Inc. The NPs were spin-coated onto the substrates, and then the substrates were heated at 100 °C for a few minutes to dry.

We thank R. Bratschitsch for helpful discussions. We also gratefully acknowledge financial support from the following sources: NSF DMR-0747822, ONR N00014-08-1-0745, Welch Foundation F-1662, Texas-ARP 003658-0160-2007, and the Alfred P. Sloan Foundation. DCR acknowledges a fellowship from the NSF-IGERT program *via* grant DGE-0549417.

REFERENCES AND NOTES

1. Stroscio, J. A.; Eigler, D. M. Atomic and Molecular Manipulation with the Scanning Tunneling Microscope. *Science* **1991**, *254*, 1319–1326.
2. Eigler, D. M.; Schweizer, E. K. Positioning Single Atoms with a Scanning Tunnelling Microscope. *Nature* **1990**, *344*, 524–526.
3. Manoharan, H. C.; Lutz, C. P.; Eigler, D. M. Quantum Mirages Formed by Coherent Projection of Electronic Structure. *Nature* **2000**, *403*, 512–515.
4. Sugimoto, Y.; Abe, M.; Hirayama, S.; Oyabu, N.; Custance, O.; Morita, S. Atom Inlays Performed at Room Temperature Using Atomic Force Microscopy. *Nat. Mater.* **2005**, *4*, 156–159.
5. Sugimoto, Y.; Pou, P.; Custance, O.; Jelinek, P.; Abe, M.; Perez, R.; Morita, S. Complex Patterning by Vertical Interchange Atom Manipulation Using Atomic Force Microscopy. *Science* **2008**, *322*, 413–417.
6. Oyabu, N.; Custance, Ó.; Yi, I.; Sugawara, Y.; Morita, S. Mechanical Vertical Manipulation of Selected Single Atoms by Soft Nanoindentation Using Near Contact Atomic Force Microscopy. *Phys. Rev. Lett.* **2003**, *90*, 176102.
7. Urzhumov, Y. A.; Shvets, G.; Fan, J. A.; Capasso, F.; Brandl, D.; Nordlander, P. Plasmonic Nanoclusters: A Path Towards Negative-Index Metafluids. *Opt. Express* **2007**, *15*, 14129–14145.
8. Requicha, A. A. G. Nanomanipulation with the Atomic Force Microscope. In *Nanotechnology*; Waser, R., Ed.; Wiley-VCH: Weinheim, Germany, 2008; Vol. 3, pp 239−273.
9. Ramachandran, T. R.; Baur, C.; Bugacov, A.; Madhukar, A.; Koel, B. E.; Requicha, A.; Gazen, C. Direct and Controlled Manipulation of Nanometer-Sized Particles Using the Noncontact Atomic Force Microscope. *Nanotechnology* **1998**, *9*, 237–245.
10. Kim, Y.; Lieber, C. M. Machining Oxide Thin Films with an Atomic Force Microscope: Pattern and Object Formation on the Nanometer Scale. *Science* **1992**, *257*, 375–377.
11. Luthi, R.; Meyer, E.; Haefke, H.; Howald, L.; Gutmannsbauer, W.; Guntherodt, H. J. Sled-Type Motion on the Nanometer Scale: Determination of Dissipation and Cohesive Energies of C60. *Science* **1994**, *266*, 1979–1981.
12. Schaefer, D. M.; Reifenberger, R.; Patil, A.; Andres, R. P. Fabrication of Two-Dimensional Arrays of Nanometer-Size Clusters with the Atomic Force Microscope. *Appl. Phys. Lett.* **1995**, *66*, 1012–1014.
13. Hertel, T.; Martel, R.; Avouris, P. Manipulation of Individual Carbon Nanotubes and Their Interaction with Surfaces. *J. Phys. Chem. B* **1998**, *102*, 910–915.
14. Decossas, S.; Mazen, F.; Baron, T.; Brémond, G.; Souifi, A. Atomic Force Microscopy Nanomanipulation of Silicon Nanocrystals for Nanodevice Fabrication. *Nanotechnology* **2003**, *14*, 1272–1278.
15. Hsieh, S.; Meltzer, S.; Wang, C. R. C.; Requicha, A. A. G.; Thompson, M. E.; Koel, B. E. Imaging and Manipulation of Gold Nanorods with an Atomic Force Microscope. *J. Phys. Chem. B* **2002**, *106*, 231–234.
16. Chen, H.; Xi, N.; Li, G. CAD-Guided Automated Nanoassembly Using Atomic Force Microscopy-Based Nonrobotics. *ASE, IEEE Trans.* **2006**, *3*, 208–217.
17. Junno, T.; Deppert, K.; Montelius, L.; Samuelson, L. Controlled Manipulation of Nanoparticles with an Atomic Force Microscope. *Appl. Phys. Lett.* **1995**, *66*, 3627–3629.
18. Baur, C.; Bugacov, A.; Koel, B. E.; Madhukar, A.; Montoya, N.; Ramachandran, T. R.; Requicha, A. A. G.; Resch, R.; Will, P. Nanoparticle Manipulation by Mechanical Pushing: Underlying Phenomena and Real-Time Monitoring. *Nanotechnology* **1998**, *9*, 360–364.
19. Miyazaki, H.; Sato, T. Mechanical Assembly of Three-Dimensional Microstructures from Fine Particles. *Adv Robotics* **1997**, *11*, 169–185.
20. Yu, M.; Dyer, M. J.; Skidmore, G. D.; Rohrs, H. W.; Lu, X.; Ausman, K. D.; Ehr, J. R. V.; Ruoff, R. S. Three-Dimensional Manipulation of Carbon Nanotubes under a Scanning Electron Microscope. *Nanotechnology* **1999**, *10*, 244–252.
21. Fukuda, T.; Arai, F.; Dong, L. X. Assembly of Nanodevices with Carbon Nanotubes through Nanorobotic Manipulations. *Proc. IEEE* **2003**, *91*, 1803–1818.
22. Ritter, C.; Heyde, M.; Schwarz, U. D.; Rademann, K. Controlled Translational Manipulation of Small Latex Spheres by Dynamic Force Microscopy. *Langmuir* **2002**, *18*, 7798–7803.
23. Dieterich, J. H. Time-Dependent Friction and the Mechanics of Stick-Slip. *Pure Appl. Geophys.* **1978**, *116*, 790–806.
24. The particular value of threshold scanning rate in the first example does not apply generally. The control parameters for nanomanipulation such as scanning speed, set value, gain of the AFM, and the surface contact time, are correlated with each other to some extent and critically depend on the surface roughness and termination conditions. For example, the threshold scanning rate can be lowered as the surface contact time is reduced, and the set value needs to be increased as the contact time is prolonged.
25. The first and third NPs were assembled using the new methods, the eighth NP was assembled using a combination of the two methods, and the other five NPs were assembled using the standard method. In data

presented in this report, the fast axis is typically parallel to the cantilever arm connected to the AFM tip.
26. Corwin, A. D.; de Boer, M. P. Effect of Adhesion on Dynamic and Static Friction in Surface Micromachining. *Appl. Phys. Lett.* **2004**, *84*, 2451–2453.
27. Mate, C. M. *Tribology on the Small Scale: A Bottom up Approach to Friction, Lubrication, And Wear*; Oxford University Press: Oxford; New York, 2008.
28. Green, P. F. *Kinetics, Transport, and Structure in Hard and Soft Materials;* Taylor & Francis: New York, 2005.
29. Bocquet, L.; Charlaix, E.; Ciliberto, S.; Crassous, J. Moisture-Induced Ageing in Granular Media and the Kinetics of Capillary Condensation. *Nature* **1998**, *396*, 735–737.
30. Estrin, Y.; Brechet, Y. On a Model of Frictional Sliding. *Pure Appl. Geophys.* **1996**, *147*, 745–762.
31. Tabor, D. Junction Growth in Metallic Friction: The Role of Combined Stresses and Surface Contamination. *Proc. R. Soc. A* **1959**, *251*, 378–393.
32. Riedo, E.; Levy, F.; Brune, H. Kinetics of Capillary Condensation in Nanoscopic Sliding Friction. *Phys. Rev. Lett.* **2002**, *88*, 185505.
33. Carpick, R. W.; Salmeron, M. Scratching the Surface: Fundamental Investigations of Tribology with Atomic Force Microscopy. *Chem. Rev.* **1997**, *97*, 1163–1194.
34. Johnson, K. L.; Kendall, K.; Roberts, A. D. Surface Energy and the Contact of Elastic Solids. *Proc. R. Soc. A* **1971**, *324*, 301–313.
35. Maugis, D. Adhesion of Spheres: The JKR-DMT Transition Using a Dugdale Model. *J. Colloid Interface Sci.* **1992**, *150*, 243–269.
36. Tabor, D. Surface Forces and Surface Interactions. *J. Colloid Interface Sci.* **1977**, *58*, 2–13.
37. Timoshenko, S. P.; Goodier, J. N. *Theory of Elasticity;* McGraw-Hill: New York, 1987.
38. Cottrell, A. H. *Dislocations and Plastic Flow in Crystals*; Oxford University Press: Oxford, U.K., 1953.
39. While there have been reports that NPs may move during an image acquisition, no previous study has taken advantage of the time-dependent static friction for controllable manipulation.
40. Liu, Z.; Li, Z.; Wei, G.; Song, Y.; Wang, L.; Sun, L. Manipulation, Dissection, And Lithography Using Modified Tapping Mode Atomic Force Microscope. *Microsc. Res. Tech.* **2006**, *69* (12), 998–1004.
41. Dirk, D.; Tristan, M.; Lars, J.; Harald, F.; Claudia, R.; Udo, D. S.; Andre, S. Interfacial Friction Obtained by Lateral Manipulation of Nanoparticles Using Atomic Force Microscopy Techniques. *J. Appl. Phys.* **2007**, *102*, 084306.
42. Requicha, A. A. G. Nanorobots, NEMS, and Nanoassembly. *Proc. IEEE* **2003**, *91*, 1922–1933.